drones

Article

Digital Self-Interference Cancellation for Full-Duplex UAV Communication System over Time-Varying Channels

Lu Tian, Chenrui Shi and Zhan Xu *

Key Laboratory of Modern Measurement and Control Technology, Ministry of Education, Beijing Information Science and Technology University, Beijing 100101, China
* Correspondence: xuzhan@bistu.edu.cn

Abstract: Full-duplex unmanned aerial vehicle (UAV) communication systems are characterized by mobility, so the self-interference (SI) channel characteristics change over time constantly. In full-duplex UAV communication systems, the difficulty is to eliminate SI in time-varying channels. In this paper, we propose a pilot-aid digital self-interference cancellation (SIC) method. First, the pilot is inserted into the data sequence uniformly, and the time-varying SI is modeled as a linear non-causal function. Then, the time-varying SI channel is estimated by the discrete prolate spheroidal basis expansion model (BEM). The error of block edge channel estimation is reduced by cross-block interpolation. The result of channel estimation is convolved with the transmitted data to obtain the reconstructed SI, which is subtracted from the received signal to achieve SIC. The simulation results show that the SIC performance of the proposed method outperforms the dichotomous coordinate descent recursive least square (DCD-RLS) and normalized least mean square (NLMS) algorithms. When the interference to noise ratio (INR) is 25 dB, the performance index normalized least mean square (NMSE) is reduced by 5.5 dB and 4 dB compared with DCD-RLS and NLMS algorithms, which can eliminate SI to the noise floor, and the advantage becomes more obvious as the INR increases.

Keywords: UAV communication; full-duplex; self-interference cancellation; time-varying channel; BEM

Citation: Tian, L.; Shi, C.; Xu, Z. Digital Self-Interference Cancellation for Full-Duplex UAV Communication System over Time-Varying Channels. *Drones* **2023**, *7*, 151. https://doi.org/10.3390/drones7030151

Academic Editor: Vishal Sharma

Received: 15 January 2023
Revised: 9 February 2023
Accepted: 20 February 2023
Published: 22 February 2023

1. Introduction

Unmanned aerial vehicle (UAV) communications and networks have been extensively researched, and benefiting from their mobility and ease of deployment, UAVs have many applications [1,2], such as smart farming, high-altitude delivery, disaster rescue, etc. The wireless applications of UAVs mainly include the following forms: A UAV can be deployed as an airborne platform to extend network coverage [3,4]; as an aerial vehicle, various communication equipment can be loaded onto the UAV, and a line-of-sight (LoS) communication link can be established with the ground terminal due to few obstacles in the air. Another use is the dissemination and collection of data [5], for example, in precision agriculture applications; a UAV is sent to disseminate (or collect) delay-tolerant information to (from) a large number of distributed wireless devices. The last one is UAV-aided relaying, for example, in emergency rescue [6]; a UAV can be deployed between the frontline and the command center to provide wireless connectivity between users.

With the commercialization of fifth generation mobile network (5G) technology, the growing number of users and demand, and the rapid development of various emerging technologies, researchers have started to conduct research related to sixth generation mobile network (6G) technology. In the 6G communication environment, a large amount of data needs to be transmitted over wireless networks [7], and a space–air–ground–sea integration network (as shown in Figure 1) will be one of the key research directions of 6G [8]. Due to their mobility, autonomy, and maneuverability, UAV platforms will be one of the most prominent infrastructures in airborne communication platforms [9–11], and the integration of UAVs into wireless communication is expected to play an important role in 6G [12,13].

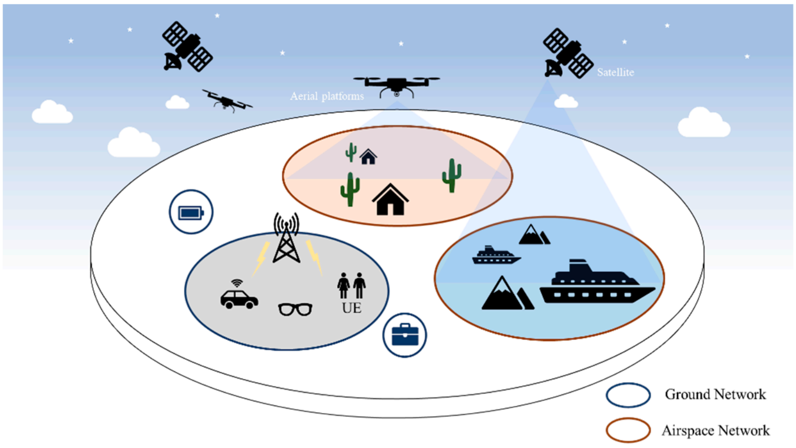

Figure 1. Space–air–ground–sea integration network.

In the 6G communication environment, the number of wirelessly connected terminals is increasing dramatically [14,15]. However, spectrum resources are on the verge of scarcity, and existing wireless communication networks usually use half-duplex technology, with each user's uplink and downlink channels occupying separate time-frequency resources, which results in the already scarce wireless spectrum resources being far from fully utilized. To improve the throughput of the communication system, the spectrum utilization of the communication system must be improved [16,17]. Full-duplex (FD) devices enable simultaneous transmission and reception of data in the same frequency band with doubled spectrum utilization [18,19]. To meet the required spectral efficiency of 6G wireless communication, FD is envisaged to constitute pivotal assets [20].

Since FD technology shares the transceiver frequency band, this will certainly lead to the transmit signal of the same device coupled to its receiving link triggering strong self-interference (SI) between the transceiver link, and SI is the main barrier in implementing FD (as shown in Figure 2). SI cancellation (SIC) can be performed in different domains, which are broadly classified as radio frequency (RF), analog and digital domain [21]. RF domain cancellation includes isolating the transceiver antenna [22] (passive RF cancellation) and injecting cancellation signals in the RF domain [23] (active RF cancellation). Analog SI cancellation achieves SIC by sending a counter-phase signal on the other link and combining it with the received signal at the receiving end [24]. The core idea of SIC in the digital domain is to eliminate SI by reconstructing the SI signal using the relevant techniques of digital signal processing [25]. Digital domain cancellation is the last step in self-interference cancellation. Traditional methods include least square (LS), minimum mean square error (MMSE), linear minimum mean square error, (LMMSE) and an adaptive filtering algorithm based on least mean squares (LMS). Among them, LS estimation is widely used to estimate the SI channel due to its low complexity, after reconstructing the SI and then subtracting it from the received signal to eliminate the SI. Ref. [26] modeled the nonlinear SI channel through a parallel Hammerstein model and estimated the nonlinear coefficients using the LS estimator. A widely linear digital SI canceller was developed in [27] to accurately estimate the SI signal.

The propagation characteristics of a fading wireless channel mainly include large-scale and small-scale fading characteristics, in which large-scale fading characterizes the attenuation of the average receiving power caused by the signal moving over a large distance. Small-scale fading is a complex phenomenon due to small changes in the spatial area between the transmitter and receiver, resulting in large changes in the amplitude and phase of the signal. Small-scale fading includes two mechanisms, multipath delay expansion and Doppler expansion, as shown in Figure 3.

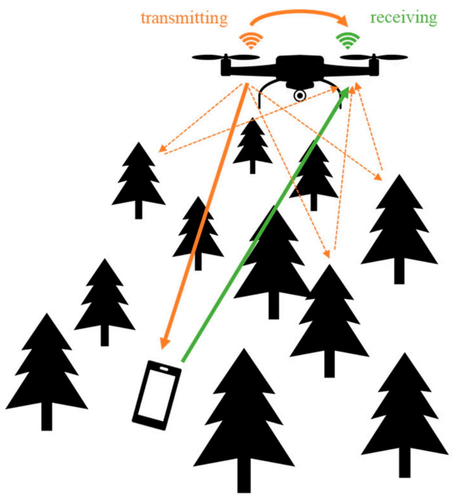

Figure 2. Formation of SI in UAV.

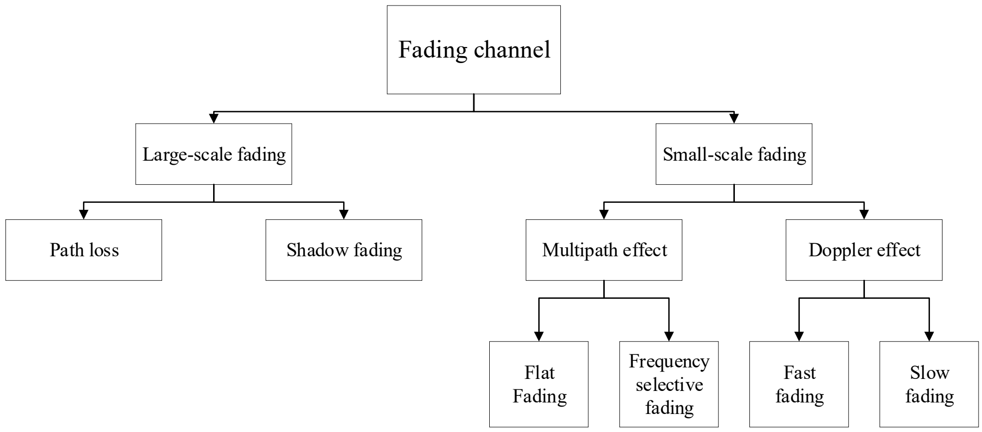

Figure 3. Channel fading.

In UAV-to-ground communications, due to the high mobility of UAVs and the presence of obstacles, the SI channel is susceptible to the Doppler effect, multipath effect, and the effect of frequently and continuously changing channel conditions, so the channel parameters will change over time [28]. In practical UAV communications scenarios, trees and tall buildings are usually around the UAVs. The time-varying component of the SI signal is generated when the received signal consists of the reflected signal. It will affect the estimation of the self-interference signal. Although the time-varying component is small, it cannot be ignored for the sake of model integrity. Few studies have been carried out on time-varying SI channels. Although the time-varying component is much smaller than the static component, the time-varying component cannot be ignored [29]. Although the authors of [29] consider the effect of time-varying SI, their research on time-varying channels is insufficient. Time-varying channels are usually modeled by using the Gauss–Markov model [30] or basis expansion model (BEM) [31]. In the Gauss–Markov model, channel variation is tracked through symbol-by-symbol updating [28]. In the BEM model, channel variation is represented by a set of time-varying basis functions. The commonly used base expansion models are complex exponential-BEM [32] (CE-BEM), polynomial-BEM [33] (P-BEM), and discrete prolate spheroidal-BEM [34] (DPS-BEM). BEM not only provides a good estimation of time-varying channel parameters but also has low computational complexity. In this paper, we improve BEM by combining it with time-varying channel characteristics and applying it to a full-duplex UAV communication system.

Traditional full-duplex self-interference channel estimation methods are limited in time-varying channels. This paper improves the cancellation performance by establishing basic expansion models. In this paper, we consider pilot-aided BEM time-varying channel estimation, we place multiple pilots in the data uniformly, and gain the basis coefficients by LS estimation using the input and output of the multiple pilots. The SI is obtained by multiplying the coefficients with the basis function of the data and then subtracting it from the received signal to complete the SIC in the digital domain. The main contribution and the novelty of the proposed research are that the coefficients of BEM are solved by establishing a linear non-causal model of the transmitted signal and uniformly interpolating the pilot, thus, the channel parameters are estimated and the self-interference signal is reconstructed. As a result, the estimation block edge error is reduced by the cross-block interpolation method, which improves the accuracy of self-interference reconstruction.

The remainder of this paper is organized as follows: Section 2 introduces the system model of digital SIC over time-varying channels in full-duplex UAV communication, and in Section 3, the proposed SIC algorithm based on BEM is derived. Simulation results are given in Section 4. Conclusions are drawn in Section 5.

2. System Model

In the full-duplex system, the transceiver antennas are shared, allowing simultaneous transmission and reception of signals in the same frequency bandwidth. However, the transmit signal can induce serious self-interference to its receiving end [17].

In the full duplex system, a complex-valued signal $s(n)$ is pulse-shaped and up-sampled, then passed through a digital-to-analog converter (DAC) and amplified in the power amplifier (PA). The received signal $y(t)$ contains the SI signal $r(t)$ together with noise $n(t)$, and the $y(n)$ is obtained through an analog-to-digital converter (ADC). The same operation is performed on the PA output, and the output $x(n)$ is used for digital self-interference cancellation. The block diagram of the digital SI cancellation is shown in Figure 4.

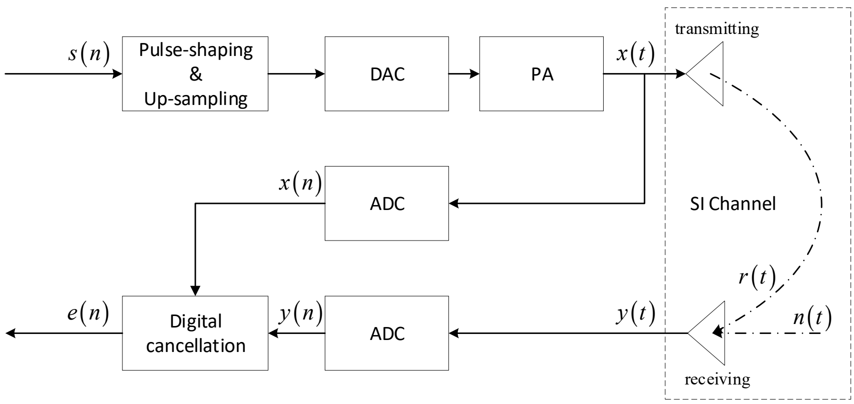

Figure 4. Block diagram of the digital SI cancellation.

In high-speed mobile scenarios, the wireless channel is susceptible to Doppler and multipath effects [35], so the channel is directly characterized by time delay and Doppler shift, and the received signal $y(t)$ can be written as

$$y(t) = \sum_{l=1}^{L} c_l x(t - \tau_l) e^{j2\pi v_l t} \tag{1}$$

where c_l, τ_l, and v_l are the fading coefficient, time delay, and Doppler shift of the l-th path, respectively. v_l is less than a specific maximum Doppler frequency offset.

The basic idea is that this part of the self-interference can be modeled as a linear and non-causal function of the transmitted signal [36]. Since the transmit data sequence is known, we can use transmission data from the future to estimate the self-interference at the current instant. In other words, the received sample $y[n]$ at any instant can be modeled as a linear combination of multiple samples of a known transmit sequence $x[n]$ before and after instant n. Thus, the discrete-time baseband equivalent of the SI symbols received at instant n can be written as

$$y(n) = x(n-k)h(k) + x(n-k+1)h(k-1) + \cdots + x(n+k-1)h(-k+1) + w(n) \quad (2)$$

where $h(k), \cdots, h(-k+1)$ represents the attenuations applied by the channel to the transmitted function in the assumed non-causal system, and $w(n)$ is complex additive white Gaussian noise (AWGN).

Let the received samples be $y[0], \ldots, y[n]$. Then the above channel equations can be written as

$$y = Ah + w \quad (3)$$

where A is Toeplitz matrix

$$A = \begin{pmatrix} x(-k) & \cdots & x(0) & \cdots & x(k-1) \\ \cdots & \cdots & \cdots & \cdots & \cdots \\ x(n-k) & \cdots & x(n) & \cdots & x(n+k-1) \end{pmatrix} \quad (4)$$

We consider a block transmission design where the pilot symbols are multiplexed with the data by periodically placing them in the block, as shown in Figure 5. In Figure 5, the transmission block consists of sub-blocks, each containing a data sub-block and a pilot sub-block. The data cluster in each sub-block has L leading zero clusters and L trailing zero clusters, and this structure can effectively suppress inter-code interference. In the Figure 4, although the transmit signal and the receive signal are divided into multiple parts, their relationships can all be expressed in terms Equations (3) and (4).

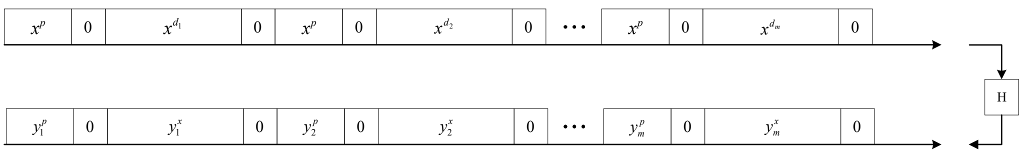

Figure 5. The frame structure of the transceiver signal.

In this paper, the Zadoff–Chu (ZC) sequence is inserted into the transmit signal as a pilot for SI channel estimation. The ZC sequence is a complex sequence, defined by

$$x(n) = \begin{cases} \exp \frac{j\pi r n^2}{N} & for\ even\ N \\ \exp \frac{j\pi r n(n+1)}{N} & for\ odd\ N \end{cases} \quad (5)$$

where, N is the length of the ZC sequence, $n = 0, 1, \ldots, N-1$, $j^2 = -1$, and r is the root index relatively prime to N.

The sequence possesses an ideal autocorrelation property, constant amplitude property, and low peak-to-average power ratio (PAPR) property. Moreover, it possesses reflexivity, i.e., $x(N-n) = x(n)$.

3. Self-Interference Cancellation

3.1. Basis Expansion Model

For a time-varying channel, the time-varying characteristics of the channel can be characterized accurately by using the basis expansion model, so the basis expansion model is used to simulate the channel. BEM is commonly deployed to approximate parameters of the time-varying channel with a decomposition over a set of elementary functions [37].

$$h_l(n) = \sum_{m=0}^{M-1} b_{lm} \cdot B_m(n) \qquad l = 0, \cdots, L-1; n = 0, \cdots, K-1 \quad (6)$$

where, $h_l(n)$ denotes the l-th memory component of the channel impulse response, b_{lm} is the coefficient of BEM, and M is the number of bases, B represents a set of basis functions, and B_m is one of them. It is assumed that does not vary with n in the period K. In other words, we consider that the time-varying channel parameters are projected onto M different time-varying basisduring the period K, and the coefficients are time-invariant. However, b_{lm} is varied in different periods K.

The common basis functions are the complex exponential basis, polynomial basis, discrete prolate spheroidal basis, etc. The discrete prolate spheroidal basis is a series of orthogonal spherical functions. It adopts a rectangular power spectrum and has strong energy concentration, which can be approximately applicable to all channel characteristics. In this paper, the discrete prolate spheroidal basis is chosen, which is the eigenvector of the autocorrelation matrix of the channel impulse response. It is assumed that the autocorrelation function of the l-th path can be expressed as

$$R_l = E\{h(n;l)h^*(m;l)\} = \sigma_l^2 \frac{\sin[2\pi(n-m)f_{d_{\max}}T_s]}{\pi(n-m)} \tag{7}$$

where, σ_l^2 is the power of the l-th path. The singular value decomposition is used to decompose R_l.

$$R_l = U_l \Lambda_l U_l^H \tag{8}$$

where Λ_l is a diagonal matrix, and the elements are the eigenvalues of R_l arranged from largest to smallest. U_l is the matrix of eigenvectors corresponding to each eigenvalue. Take the first M columns of U_l as the basis function

$$B = U_l(:, 1:M) \tag{9}$$

In the simulation, the change in the mobile terminal speed will cause a change in the Doppler expansion, which will affect the accuracy of the BEM to estimate the channel. The carrier frequency is 1.5 GHz, the signal bandwidth is 200 K, and the velocity of the mobile terminal is changed from 100 m/s to 500 m/s. The estimation accuracy is expressed as the mean square error (MSE). The simulation result of the channel estimation is shown in Figure 6. It is observed that the SIC performance of the DPS-BEM is better than CE-BEM and P-BEM.

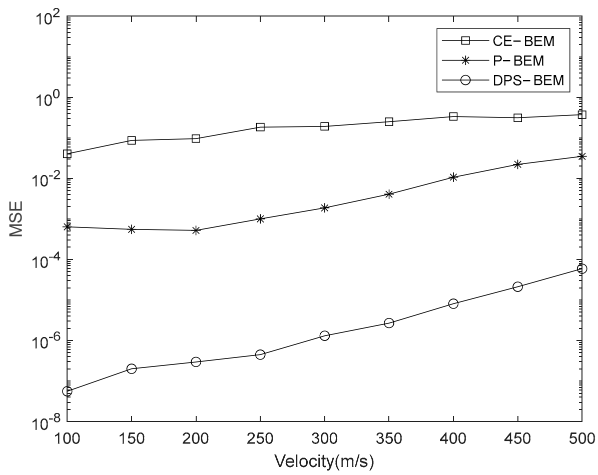

Figure 6. Channel estimation performance of different basis functions.

When the number of basis functions is 1, the BEM channel estimation degenerates into LS channel estimation. However, it is not better to have more basis functions; the more basis function, the more oscillations are easily caused at the pilot, which makes the overall estimation performance worse and increases the computational effort. Figure 7 shows the relationship between the number of basis functions and the SI cancellation performance.

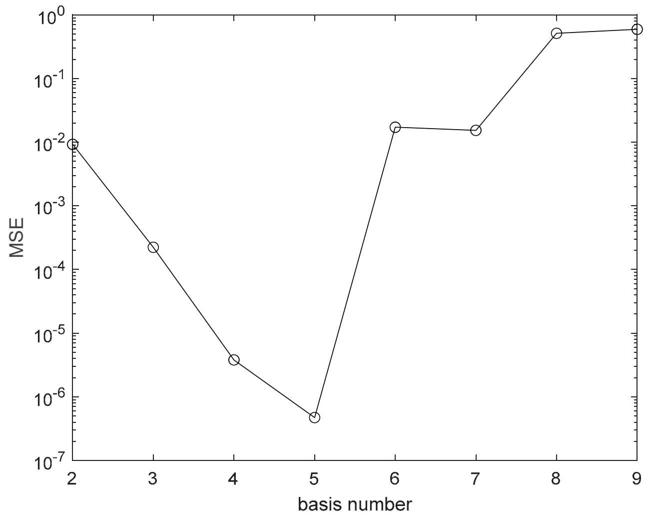

Figure 7. Effect of the number of basis function on channel estimation performance.

When the sampling frequency is f_s , and the Doppler shift is f_d , the period of the frequency component (i.e., the frequency component of time-selective fading) generated by Doppler shift is approximately $1/f_d$, and the number of data samples is approximately f_s/f_d in this period.

3.2. Proposed BEM SIC Algorithm

The block diagram of the proposed BEM SIC algorithm is shown in Figure 8. Without loss of generality, consider a transmitting block including m pilots. We thus deploy a widely used discrete prolate spheroidal BEM. For the pilot in the block, its corresponding received signals can be expressed as

$$\mathbf{y}_p{=}\mathbf{A}_p\mathbf{h}_p + \mathbf{w} \tag{10}$$

where $\mathbf{y}_p = \left[\mathbf{y}_1^T, \ldots, \mathbf{y}_{m_p}^T\right]^T$, $\mathbf{y}_{m_p}$ is the corresponding received signals of $m_p -$ th transmitting pilot. $\mathrm{A}_p = \left[\mathrm{A}_1^T, \ldots, \mathbf{A}_{m_p}^T\right]^T$, A_{m_p} is the matrix formed by $m_p -$ th transmitting pilot according to (4), and $\mathbf{A}_p$ has a total of n_p rows. $\mathbf{h}_p = \left[\mathbf{h}_1^T, \ldots, \mathbf{h}_{m_p}^T\right]^T$, $\mathbf{h}_{m_p}$ is the channel impulse response when the $m_p -$ th pilot is sent.

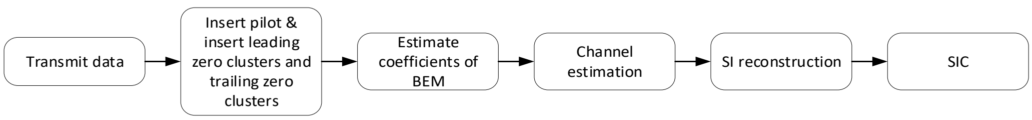

Figure 8. System block diagram.

The corresponding received signals based on BEM can be represented as

$$\begin{aligned}
\mathbf{y} &= diag\{\mathbf{AbB} + \mathbf{w}\} \\
&= diag\left\{ \mathbf{A} \begin{pmatrix} b_{k,1} & \cdots & b_{k,m} \\ \vdots & \ddots & \vdots \\ b_{-k+1,1} & \cdots & b_{-k+1,m} \end{pmatrix} \begin{pmatrix} \mathbf{B}_1 \\ \vdots \\ \mathbf{B}_m \end{pmatrix} + \mathbf{w} \right\} \\
&= \begin{pmatrix} \mathbf{A}_{1,j}B_1(1) & \cdots & \mathbf{A}_{1,j}B_m(1) \\ \vdots & \ddots & \vdots \\ \mathbf{A}_{n_p,j}B_1(n_p) & \cdots & \mathbf{A}_{n_p,j}B_m(n_p) \end{pmatrix} \begin{pmatrix} \mathbf{b}_1 \\ \vdots \\ \mathbf{b}_m \end{pmatrix} + \mathbf{w} \\
&= \bar{\mathbf{A}}\mathbf{b}' + \mathbf{w}
\end{aligned} \tag{11}$$

where, $\mathbf{b} = (\mathbf{b}_1, \ldots, \mathbf{b}_m)$, $\mathbf{B} = \left(\mathbf{B}_1^T, \ldots, \mathbf{B}_m^T\right)^T$, $\mathbf{B}_m$ is the sampled value of the m-th basis function at all pilots in the block. $\mathbf{b}_m$ is the coefficient of the m-th basis function in all paths.

To obtain an estimate $\hat{\mathbf{b}}'$ of the coefficients $\mathbf{b}'$, this paper adopts LS estimation with the objective of minimizing the cost function (12)

$$\begin{aligned} \mathrm{J}\left(\hat{\mathbf{b}}'\right) &= \left\| \mathbf{y} - \bar{\mathbf{A}}\hat{\mathbf{b}}' \right\|^2 \\ &= \left(\mathbf{y} - \bar{\mathbf{A}}\hat{\mathbf{b}}'\right)^H \left(\mathbf{y} - \bar{\mathbf{A}}\hat{\mathbf{b}}'\right) \\ &= \mathbf{y}^H\mathbf{y} - \mathbf{y}^H\bar{\mathbf{A}}\hat{\mathbf{b}}' - \hat{\mathbf{b}}'^H\bar{\mathbf{A}}^H\mathbf{y} + \hat{\mathbf{b}}'^H\bar{\mathbf{A}}^H\bar{\mathbf{A}}\hat{\mathbf{b}}' \end{aligned} \tag{12}$$

By setting the derivative of the Equation (12) with respect to $\hat{\mathbf{b}}'$ to zero,

$$\frac{\partial J\left(\hat{\mathbf{b}}'\right)}{\partial \hat{\mathbf{b}}'} = -2\left(\bar{\mathbf{A}}^H\mathbf{y}\right)^* + 2\left(\bar{\mathbf{A}}^H\bar{\mathbf{A}}\hat{\mathbf{b}}'\right)^* = 0 \tag{13}$$

we have $\bar{\mathbf{A}}^H\mathbf{y} = \bar{\mathbf{A}}^H\bar{\mathbf{A}}\hat{\mathbf{b}}'$, which gives the solution to the LS estimation as

$$\hat{\mathbf{b}}'_{LS} = \left(\bar{\mathbf{A}}^H\bar{\mathbf{A}}\right)^{-1}\bar{\mathbf{A}}^H\mathbf{y} \tag{14}$$

where $\hat{\mathbf{b}}'_{LS} = \left[\hat{\mathbf{b}}_1^T, \ldots, \hat{\mathbf{b}}_m^T\right]^T$.

The basic structure of the proposed algorithm is shown in Figure 9. In summary, the BEM coefficients are obtained by the LS estimation using the transceiver signals at the pilot position. Then, self-interference signals are estimated by multiplying the transmitted signal with the basis coefficients and the basis function. Finally, the self-interference cancellation is completed by subtracting it from the receiving end.

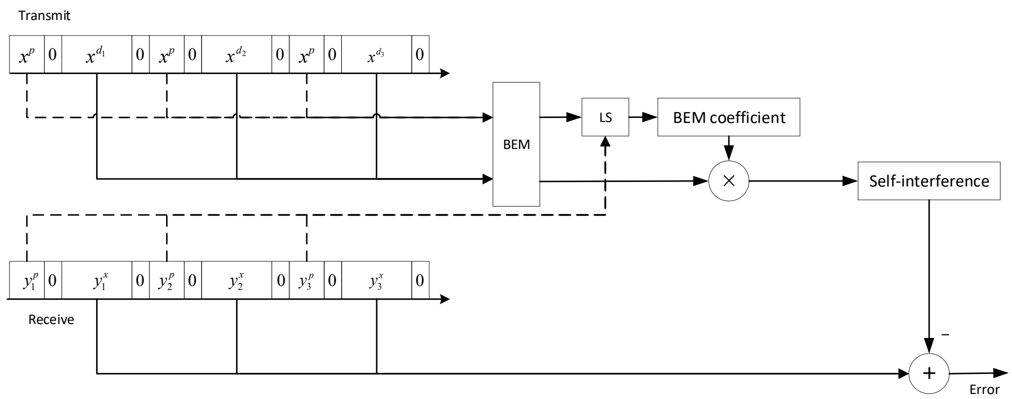

Figure 9. The basic structure of the proposed algorithm.

We consider that the coefficients of the basis function are constant in the block. It is easy to obtain the estimated value $\hat{y}(n)$ of the SI signal at receiver, according to Equation (3), by using the sampling value of the basis function at the instant of transmitted data. After the SI signal is reconstructed, it is then subtracted from the received signal to obtain the error signal $e(n)$.

$$\begin{aligned} e(n) &= y(n) - \hat{y}(n) \\ &= y(n) - x(n-k)\hat{h}(k) - x(n-k+1)\hat{h}(k-1) - \cdots - x(n+k-1)\hat{h}(-k+1) \end{aligned} \tag{15}$$

The normalized mean square error (NMSE) is often used to evaluate the performance of channel estimation, and this paper evaluates the performance of SI cancellation by comparing the NMSE in logarithmic form.

$$\text{NMSE} = 10\log_{10}\left\{E\left\{|e(n)|^2\right\}/E\left\{|y(n)|^2\right\}\right\} \tag{16}$$

A drawback of block-based transmission is that the channel estimation and bit errors are more concentrated toward the block edges. This may be because of the rectangular windowing, which essentially distorts the effective channel towards the edges [38]. Through simulations, it is observed that the errors are more concentrated toward both ends of the transmission block.

To solve this problem, when the channel parameters of the current block are estimated, the last pilot in the previous block and the first pilot in the following block is additionally used for interpolation estimation, as shown in Figure 10.

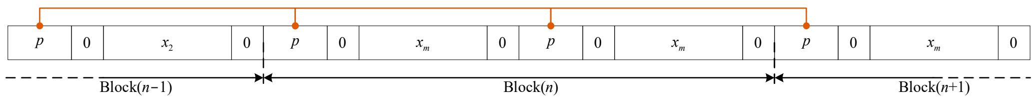

Figure 10. Cross-block estimation structure.

4. Simulation Results

In this section, we discuss the simulation results for the proposed BEM algorithm over time-varying channels. The specific parameters of the full duplex model are as follows: The bandwidth of the transmitted signal is 200 KHz, the carrier frequency is 1.5 GHz, the sampling rate is 3.2 MHz, and uncoded 16 quadrature amplitude modulation (16 QAM) is used. We set the received signal strength very small. The SNR is close to 0 dB. It is assumed that the speed of UVA is 100 m/s, so the maximum Doppler shift is 500 Hz. We establish the time-varying channel through the comm.RayleighChannel() function in MATLAB. When comparing different algorithms in simulation, appropriate parameters are set to ensure that each estimated self-interference signal time is within the correlation time. The proposed algorithm in this paper is analyzed and compared with the classical recursive least square (RLS) algorithm and LMS algorithm, which are commonly used for digital self-interference cancellation.

First, we optimize the parameters of the model for the proposed SIC method. The parameters are memory length, pilot length and the number of sub-blocks in a block. When the effect of a parameter on the SIC performance is considered, the rest of the parameters will be set in the appropriate range. The simulated SI channel is set as a multipath time-varying channel. The number of multipaths is three and the delays are [0, 2×10^{-6}, 5×10^{-6}] seconds and the powers are $[0, -21, -41]$ dB. It is assumed that the INR of the receiver is 25 dB.

In this paper, the SI is modeled as a linear and non-causal function of the transmitted signal. In other words, it is assumed that the SI at the current instant is related to the transmitted signals before and after the current instant. So, the elimination effect of SI is related to the memory length, and Figure 11 shows their relationship (the length refers to the forward memory length only and the backward memory length is equal to the forward memory length). When the memory length increases to 4, the improvement of SIC is no longer significant.

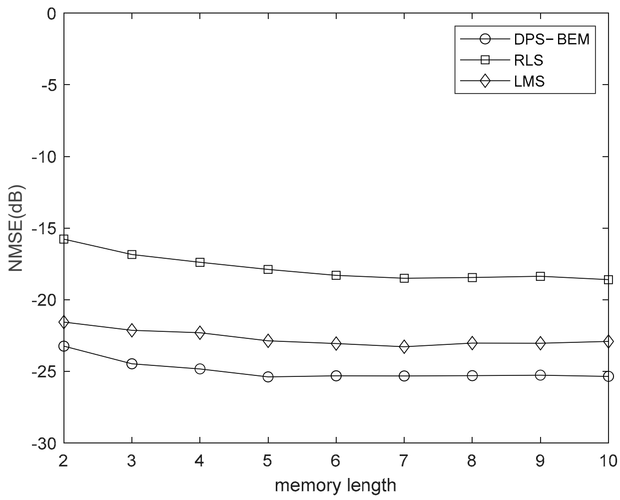

Figure 11. Effect of memory length on SIC performance.

As the pilot in the sub-block grows, the performance of channel estimation will be more accurate and the SIC performance will be better, but this will lead to inefficient data transmission. Figure 12 shows the relationship between the pilot length and the SIC performance, and when the pilot length is between 20 and 30, the SI can be eliminated near the noise floor.

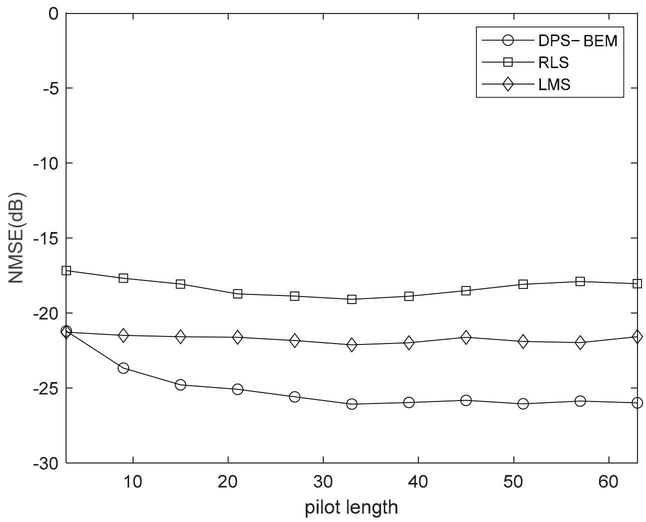

Figure 12. Effect of pilot length on SIC performance.

The number of sub-blocks in a block affects the performance of channel estimation and thus the SIC performance. Figure 13 shows the relationship between the number of sub-blocks and the SIC performance; we can see that when the number of sub-blocks increases to 4, the SIC performance is no longer obvious, and as the number of sub-blocks increases, it will lead to a reduction in data transmission efficiency.

In the simulation, the memory length is 4, the pilot length is 21, and a block includes four sub-blocks. The proposed algorithm is analyzed and compared with the DCD-RLS and NLMS algorithm from [39]. NLMS and DCD-RLS increase the convergence rate by setting the step size to a variable over time. DCD-RLS also reduces computational complexity. With their superior performance, these two algorithms are also commonly used in digital self-interference cancellation systems. The SI channel in Figure 14 is a single-path and time-varying channel, where the path is in accord with the Rayleigh distribution. The SI channel in Figure 15 is multi-path and time-varying channel, where each path is in accord with the Rayleigh distribution. It can be seen that the SIC performance of the proposed algorithm is better than the classical RLS and NLMS algorithms, which can effectively eliminate the SI to the noise floor, and as the INR is bigger, this superiority is clearer.

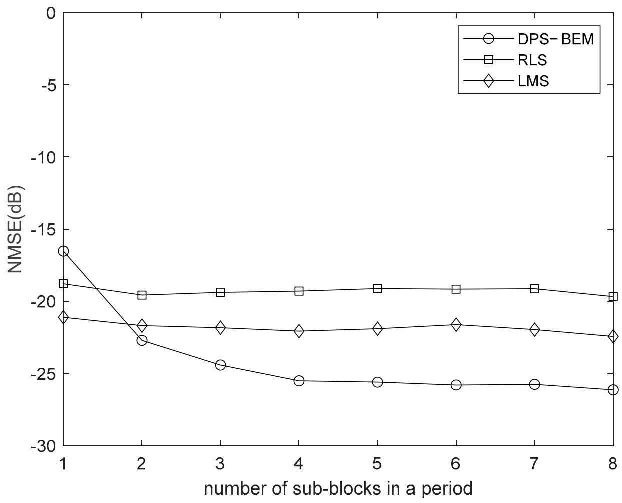

Figure 13. Effect of the number of sub-blocks on SIC performance.

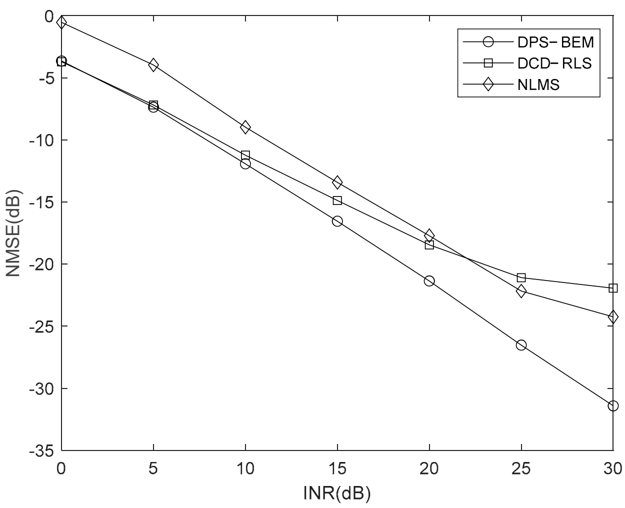

Figure 14. SIC performance over single-path and time-varying channel.

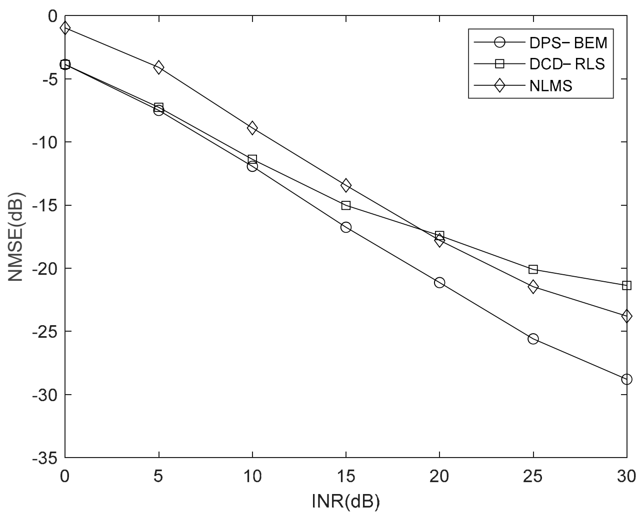

Figure 15. SIC performance over multipath and time-varying channel.

Finally, we analyze the effect of terminal movement speed on the SIC performance of the algorithm through simulation. In the simulation, we set INR as 25 dB. The results are shown in Figure 16. It can be seen that the proposed algorithm still has a high SIC performance as the terminal moves faster.

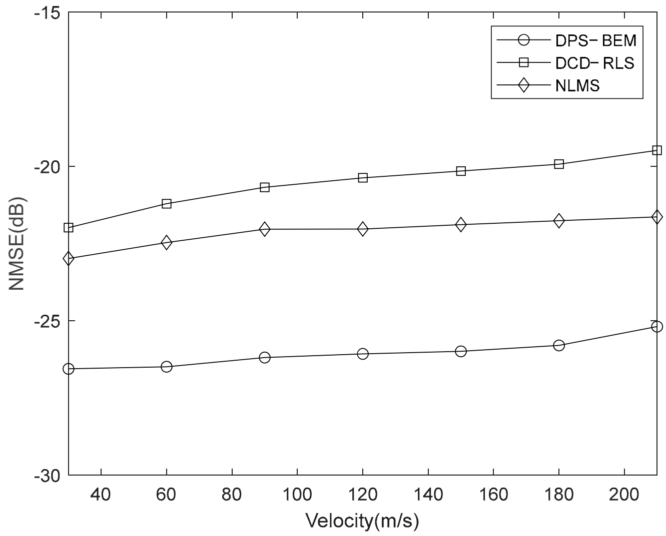

Figure 16. Effect of velocity on SIC performance.

5. Conclusions

In this article, we investigated a digital cancellation method for time-varying SI in a full-duplex UAV communication system. We model the time-varying SI by a linear non-causal function and eliminate the digital SI by DPS-BEM. Moreover, the error at the block edge is reduced by interpolation cross-block, and the SI in the time-varying channel is eliminated effectively. The simulation results show that the SIC of the proposed method has a better performance compared with the DCD-RLS and NLMS algorithm. For example, when the INR is 25 dB, the performance index NMSE is reduced by 5.5 dB and 4 dB compared with DCD-RLS and NLMS algorithms, respectively, which can effectively eliminate SI to the noise floor, and the advantage becomes more obvious as the INR increases. Moreover, with the change of terminal moving speed, the proposed algorithm always has a good self-interference cancellation performance. In future work, we will consider the effect of nonlinear SI over time-varying channels and do research in the analogy domain.

Author Contributions: Conceptualization, L.T. and Z.X.; methodology, L.T. and C.S.; software, C.S.; validation, L.T. and Z.X.; formal analysis, L.T.; investigation, C.S.; resources, Z.X.; writing—original draft preparation, C.S.; writing—review and editing, L.T.; visualization, C.S.; supervision, L.T.; project administration, Z.X.; funding acquisition, L.T. All authors have read and agreed to the published version of the manuscript.

Funding: This research received was funded in part by National Natural Science Foundation of China under Grant 62201070, and in part by the Science and Technology Project of the Beijing Municipal Education Commission under Grant KM202211232009.

Data Availability Statement: No new data were created or analyzed in this study. Data sharing is not applicable to this article.

Conflicts of Interest: The authors declare no conflict of interest.

References

1. Chen, C.; Chen, S.; Hu, G.; Chen, B.; Chen, P.; Su, K. An auto-landing strategy based on pan-tilt based visual servoing for unmanned aerial vehicle in GNSS-denied environments. *Aerosp. Sci. Technol.* **2021**, *116*, 106891. [CrossRef]
2. Song, B.D.; Park, K.; Kim, J. Persistent UAV delivery logistics: MILP formulation and efficient heuristic. *Comput. Ind. Eng.* **2018**, *120*, 418–428. [CrossRef]

3. Liu, X.; Li, Z.; Zhao, N.; Meng, W.; Gui, G.; Chen, Y.; Adachi, F. Transceiver Design and Multihop D2D for UAV IoT Coverage in Disasters. *IEEE Internet Things J.* **2018**, *6*, 1803–1815. [CrossRef]
4. Shi, M.; Yang, K.; Niyato, D.; Yuan, H.; Zhou, H.; Xu, Z. The meta distribution of SINR in UAV-assisted cellular networks. *IEEE Trans. Commun.* **2023**, *71*, 1193–1206. [CrossRef]
5. Cheng, F.; Gui, G.; Zhao, N.; Chen, Y.; Tang, J.; Sari, H. UAV-Relaying-Assisted Secure Transmission with Caching. *IEEE Trans. Commun.* **2019**, *67*, 3140–3153. [CrossRef]
6. Bouachir, O.; Aloqaily, M.; Garcia, F.; Larrieu, N.; Gayraud, T. Testbed of QoS Ad-Hoc Network Designed for Cooperative Multi-drone Tasks. In Proceedings of the 17th ACM International Symposium on Mobility Management and Wireless Access, Miami Beach, FL, USA, 25–29 November 2019; pp. 89–95. [CrossRef]
7. Alsamhi, S.H.; Almalki, F.A.; Ma, O.; Ansari, M.S.; Lee, B. Predictive Estimation of Optimal Signal Strength from Drones Over IoT Frameworks in Smart Cities. *IEEE Trans. Mob. Comput.* **2021**, *22*, 402–416. [CrossRef]
8. Dai, H.N.; Wu, Y.; Imran, M.; Nasser, N. Integration of Blockchain and Network Softwarization for Space-Air-Ground-Sea Integrated Networks. *IEEE Internet Things Mag.* **2022**, *5*, 166–172. [CrossRef]
9. Noor, F.; Khan, M.; Al-Zahrani, A.; Ullah, I.; Al-Dhlan, K. A Review on Communications Perspective of Flying Ad-Hoc Networks: Key Enabling Wireless Technologies, Applications, Challenges and Open Research Topics. *Drones* **2020**, *4*, 65. [CrossRef]
10. Alsamhi, S.H.; Shvetsov, A.V.; Kumar, S.; Hassan, J.; Alhartomi, M.A.; Shvetsova, S.V.; Sahal, R.; Hawbani, A. Computing in the Sky: A Survey on Intelligent Ubiquitous Computing for UAV-Assisted 6G Networks and Industry 4.0/5.0. *Drones* **2022**, *6*, 177. [CrossRef]
11. Chen, C.; Xiang, J.; Ye, Z.; Yan, W.; Wang, S.; Wang, Z.; Chen, P.; Xiao, M. Deep Learning-Based Energy Optimization for Edge Device in UAV-Aided Communications. *Drones* **2022**, *6*, 139. [CrossRef]
12. Zeng, Y.; Wu, Q.; Zhang, R. Accessing from the Sky: A Tutorial on UAV Communications for 5G and beyond. *Proc. IEEE* **2019**, *107*, 2327–2375. [CrossRef]
13. Amponis, G.; Lagkas, T.; Zevgara, M.; Katsikas, G.; Xirofotos, T.; Moscholios, I.; Sarigiannidis, P. Drones in B5G/6G Networks as Flying Base Stations. *Drones* **2022**, *6*, 39. [CrossRef]
14. Sodhro, A.H.; Pirbhulal, S.; Luo, Z.; Muhammad, K.; Zahid, N.Z. Toward 6G architecture for energy-efficient communication in IoT-enabled smart automation systems. *IEEE Internet Things J.* **2020**, *8*, 5141–5148. [CrossRef]
15. Almalki, F.; Soufiene, B.; Alsamhi, S.; Sakli, H. A Low-Cost Platform for Environmental Smart Farming Monitoring System Based on IoT and UAVs. *Sustainability* **2021**, *13*, 5908. [CrossRef]
16. Goyal, S.; Liu, P.; Panwar, S.; DiFazio, R.A.; Yang, R.; Li, J.; Bala, E. Improving small cell capacity with common-carrier full duplex radios. In Proceedings of the 2014 IEEE International Conference on Communications (ICC), Sydney, Australia, 10–14 June 2014; pp. 4987–4993. [CrossRef]
17. Zhang, L.; Xiao, M.; Wu, G.; Alam, M.; Liang, Y.-C.; Li, S. A Survey of Advanced Techniques for Spectrum Sharing in 5G Networks. *IEEE Wirel. Commun.* **2017**, *24*, 44–51. [CrossRef]
18. Du, C.; Zhang, Z.; Wang, X.; An, J. Optimal Duplex Mode Selection for D2D-Aided Underlaying Cellular Networks. *IEEE Trans. Veh. Technol.* **2020**, *69*, 3119–3134. [CrossRef]
19. Chai, X.; Liu, T.; Xing, C.; Xiao, H.; Zhang, Z. Throughput Improvement in Cellular Networks via Full-Duplex Based Device-to-Device Communications. *IEEE Access* **2016**, *4*, 7645–7657. [CrossRef]
20. Zhang, Z.; Long, K.; Vasilakos, A.V.; Hanzo, L. Full-Duplex Wireless Communications: Challenges, Solutions, and Future Research Directions. *Proc. IEEE* **2016**, *104*, 1369–1409. [CrossRef]
21. Panse, V.; Jain, T.K.; Sharma, P.K.; Kothari, A. Digital Self-interference cancellation in the era of machine learning: A comprehensive review. *Phys. Commun.* **2022**, *50*, 101526. [CrossRef]
22. Duarte, M.; Dick, C.; Sabharwal, A. Experiment-Driven Characterization of Full-Duplex Wireless Systems. *IEEE Trans. Wirel. Commun.* **2012**, *11*, 4296–4307. [CrossRef]
23. Jain, M.; Choi, J.I.; Kim, T.; Bharadia, D.; Seth, S.; Srinivasan, K.; Levis, P.; Katti, S.; Sinha, P. Practical, real-time, full duplex wireless. In Proceedings of the 17th Annual International Conference on Mobile Computing and Networking, Seoul, Republic of Korea, 17–21 June 2011; Association for Computing Machinery: New York, NY, USA, 2011; pp. 301–312.
24. Kim, D.; Ju, H.; Park, S.; Hong, D. Effects of Channel Estimation Error on Full-Duplex Two-Way Networks. *IEEE Trans. Veh. Technol.* **2013**, *62*, 4666–4672. [CrossRef]
25. Tian, L.; Wang, S.; Cheng, Z.; Bu, X. All-digital self-interference cancellation in zero-IF full-duplex transceivers. *China Commun.* **2016**, *13*, 27–34. [CrossRef]
26. Anttila, L.; Korpi, D.; Syrjälä, V.; Valkama, M. Cancellation of power amplifier induced nonlinear self-interference in full-duplex transceivers. In Proceedings of the 2013 Asilomar Conference on Signals, Systems and Computers, Pacific Grove, CA, USA, 3–6 November 2013; pp. 1193–1198.
27. Korpi, D.; Anttila, L.; Syrjälä, V.; Valkama, M. Widely linear digital self-interference cancellation in direct-conversion full-duplex transceiver. *IEEEJ. Sel. Areas Commun.* **2014**, *32*, 1674–1687. [CrossRef]
28. Senol, H.; Li, X.; Tepedelenlioglu, C. Rapidly Time-Varying Channel Estimation for Full-Duplex Amplify-and-Forward One-Way Relay Networks. *IEEE Trans. Signal Process.* **2018**, *66*, 3056–3069. [CrossRef]

29. Kong, D.H.; Kil, Y.-S.; Kim, S.-H. Neural Network Aided Digital Self-Interference Cancellation for Full-Duplex Communication Over Time-Varying Channels. In Proceedings of the IEEE Transactions on Vehicular Technology 2022, Helsinki, Finland, 19–22 June 2022; Volume 71, pp. 6201–6213.
30. Arredondo, G.; Chriss, W.; Walker, E. A multipath fading simulator for mobile radio. *IEEE Trans. Veh. Technol.* **1973**, *22*, 241–244. [CrossRef]
31. Shen, L.; Zakharov, Y.; Shi, L.; Henson, B. BEM Adaptive filtering for SI cancellation in full-duplex underwater acoustic systems. *Signal Process.* **2021**, *191*, 108366. [CrossRef]
32. Zarrinkoub, H. *Understanding LTE with MATLAB: From Mathematical Modeling to Simulation and Prototyping*; Wiley Publishing: Chichester, UK, 2014.
33. Borah, D.K.; Hart, B.T. Frequency-selective fading channel estimation with a polynomial time-varying channel model. *IEEE Trans. Commun.* **1999**, *47*, 862–873. [CrossRef]
34. Qu, H.; Liu, G.; Wang, Y.; Chen, Q.; Yi, C.; Peng, J. A timedomain approach to channel estimation and equalization for the SC-FDM system. *IEEE Trans. Broadcast.* **2019**, *65*, 713–726. [CrossRef]
35. Masmoudi, A.; Le-Ngoc, T. A Maximum-Likelihood Channel Estimator for Self-Interference Cancelation in Full-Duplex Systems. *IEEE Trans. Veh. Technol.* **2015**, *65*, 5122–5132. [CrossRef]
36. Bharadia, D.; McMilin, E.; Katti, S. *Full Duplex Radios*; IEEE Press: Hong Kong, China, 2013; pp. 375–386.
37. Liao, Y.; Sun, G.; Shen, X.; Zhang, S.; Yang, X.; Zhang, X.; Yao, H.; Zhang, N. BEM-based channel estimation and interpolation methods for doubly-selective OFDM channel. In Proceedings of the IEEE International Conference on Smart Internet of Things, Xi'an, China, 17–19 August 2018; pp. 70–75.
38. Qu, F.; Yang, L. On the estimation of doubly-selective fading channels. *IEEE Trans. Wirel. Commun.* **2010**, *9*, 1261–1265. [CrossRef]
39. Shen, L.; Henson, B.; Zakharov, Y.; Mitchell, P. Digital Self-Interference Cancellation for Full-Duplex Underwater Acoustic Systems. *IEEE Trans. Circuits Syst. II Express Briefs* **2019**, *67*, 192–196. [CrossRef]